0026-895X/92/020322-09$03.00/0

MOLECULAR PHARMACOLOGY, 41:322–330

Time-, Voltage-, and State-Dependent Block by Quinidine of a Cloned Human Cardiac Potassium Channel

DIRK J. SNYDERS, KAREN M. KNOTH, STEVEN L. ROBERDS, and MICHAEL M. TAMKUN

Departments of Medicine (D.J.S.), Pharmacology (K.M.K., S.L.R., M.M.T.), and Molecular Physiology and Biophysics (M.M.T.), Vanderbilt University, Nashville, Tennessee 37232-2171

Received August 13, 1991; Accepted October 25, 1991

SUMMARY

The interaction of quinidine with a cloned human cardiac potassium channel (HK2) expressed in a stable mouse L cell line was studied using the whole-cell tight-seal voltage-clamp technique. Quinidine (20 μM) did not affect the initial sigmoidal activation time course of the current. However, it reduced the peak current and induced a subsequent decline, with a time constant of 8.2 ± 0.8 msec, to 28 ± 6% of control (at +60 mV). The concentration dependence of HK2 block at +60 mV yielded an apparent K_D of 6 μM and a Hill coefficient of 0.9. The degree of block was voltage dependent. Block increased from 0.60 ± 0.09 at 0 mV to 0.72 ± 0.06 at +60 mV with 20 μM quinidine and from 0.39 ± 0.20 to 0.48 ± 0.16 with 6 μM. Paired analysis in seven experiments with 20 μM quinidine indicated that the voltage-dependent increase in block was significant (difference, 12 ± 4%; $p < 0.001$). This voltage dependence was described by an equivalent electrical distance δ of 0.19 ± 0.02, which suggested that at the binding site quinidine experienced 19% of the applied transmembrane electrical field, referenced to the inner surface. Quinidine reduced the tail current amplitude and slowed the time course relative to control, resulting in a "crossover" phenomenon. These data indicate that 1) the charged form of quinidine blocks the HK2 channel after it opens, 2) binding occurs within the transmembrane electrical field (probably in or near the ion permeation pathway), and 3) unbinding is required before the channel can close.

Quinidine is a widely used antiarrhythmic agent. It slows conduction and prolongs action potential duration, mainly by blocking cardiac Na^+ and K^+ channels, respectively (1–4). Several studies have shown that quinidine interacts mainly with the activated or open state of cardiac Na^+ channels (5, 6). However, the mechanism of block of K^+ channels is not firmly established, although there is evidence indicating that block of a slow component of delayed rectification is mainly due to open state interactions (7, 8). The presence of multiple overlapping ionic currents in native cardiac myocytes complicates the study of drug-channel interactions. A combination of ion substitution and pharmacological dissection is required to eliminate all but the current of interest (8, 9). This procedure is valuable but limited, e.g., the use of divalent cations to block Ca^{2+} currents may modify gating properties of K^+ channels, and for the study of time-dependent drug-channel interactions it is required that any agent used in the subtraction procedure be devoid of any time-dependent effects. In order to elucidate mechanisms of ion channel block quantitatively, it is, therefore, necessary to study drug-channel interactions in a system without contaminating currents. The expression of cloned cardiac K^+ channels in tissue culture cells provides such a system. We have taken advantage of this system to study the interaction of quinidine with HK2, a K^+ channel cloned from human ventricle.

Several K^+ channels have recently been cloned from rat and human heart (10, 11). Although the 605-amino acid HK2 channel was cloned from a human ventricular cDNA library, Northern blot analysis suggests that it is much more abundant in atrium relative to ventricle (11). The RK4 channel (alternatively designated Kv1) cloned from rat heart (10) and brain (12) appears to be the rat equivalent of this human channel. The HK2 and RK4 channels are 86% identical overall, with 96% identity within the central core region containing the six membrane-spanning domains. HK2 is functionally similar to this rat channel, in that it has delayed rectifier properties, displays some degree of slow inactivation and activates positive to −30 mV, with time constants ranging from 40 msec at −20 mV to 2 msec at +50 mV (12). RK4 mRNA is expressed at equivalent levels during all stages of rat heart development

This work was supported by the Stahlman Endowment (D.J.S.) to Vanderbilt University and National Institutes of Health Grants DRR-2SO7-RR05424 (D.J.S.), HL 40608 (P. Bennett), and GM 41325 (M.M.T.) and was done during the tenure of a Grant-in-Aid award (M.M.T.) from the American Heart Association and Winthrop Pharmaceuticals. M.M.T. is an Established Investigator of the American Heart Association. K.M.K. was supported by Medical Scientist Training Program Grant GM 07347, and S.L.R. was supported by National Institutes of Health Training Grant GM 07628 and an advanced predoctoral fellowship from the Pharmaceutical Manufacturers Association Foundation.

ABBREVIATIONS: TEA, tetraethyl ammonium; HEPES, 4-(2-hydroxyethyl)-1-piperazineethanesulfonic acid; ANOVA, analysis of variance; BAPTA, 1,2-bis(2-aminophenoxy)ethane-*N*,*N*,*N*′,*N*′-tetraacetic acid.

(13), suggesting that this channel is crucial to cardiac function. Native currents similar to RK4 and HK2 have been recently described in rat atrial myocytes (14), suggesting that this channel may have an important role in the control of action potential duration and repolarization in native cardiac membranes. Interestingly, a K^+ channel cloned from human insulinoma cells is nearly identical to HK2 in both amino acid sequence (96% overall identity) and kinetic properties (15).

The HK2 channel was stably expressed in mouse L cells, and the mechanism of block by quinidine was studied using the whole-cell voltage-clamp technique. Under the experimental conditions used in this study, no contaminating voltage-activated currents were observed. Quinidine interacts primarily with the open state of the HK2 channel, and quinidine must dissociate from the channel before it can close. The voltage dependence of this open-channel block indicated that quinidine acts from the inside and moves about 19% into the membrane electrical field to reach its binding site. Despite obvious kinetic differences, quinidine blocks this human cardiac K^+ channel in a manner similar to the block of the *Drosophila Shaker* channel by internal TEA (16). This suggests that TEA and quinidine receptors are adjacent or identical structures. This work provides topological information to guide molecular strategies to identify the receptor site, because it suggests that the interaction occurs with membrane-spanning domains at or near the TEA binding site.

Materials and Methods

Transfection and cell culture. The *Sph*I-*Eco*RV fragment (base pairs 161–2059) of the HK2 cDNA (11) was blunted with Klenow and subcloned in the *Eco*RV site of pMSVNeo (17). This vector contains a dexamethasone-inducible murine mammary tumor virus promotor controlling transcription of the inserted cDNA and a gene conferring neomycin resistance driven by the SV40 early promotor. The HK2-pMSVNeo construct contained only 22 and 59 base pairs of the 5′ and 3′ untranslated sequence, respectively. The cDNA-containing expression vector was transfected into mouse *Ltk*$^-$ cells as described previously (18). After 24 hr, selection with 0.5 mg/ml G418 (a neomycin analog) was initiated for 2 weeks or until discrete foci formed. Individual foci were isolated, maintained in 0.25 mg/ml G418, and screened for HK2 mRNA by Northern analysis. Each of 10 cell lines examined for HK2 mRNA were positive. The two of these lines with the highest levels of HK2 mRNA were chosen for further study. Both lines had equivalent HK2 channel expression, as determined by current density in whole-cell voltage clamp. One of the lines was chosen for further detailed analysis.

Transfected cells were cultured in Dulbecco's modified Eagle medium supplemented with 10% horse serum and 0.25 mg/ml G418, under a 5% CO_2 atmosphere. The cultures were passed every 3–5 days, using a brief trypsin treatment. Before experimental use, subconfluent cultures were incubated with 2 μM dexamethasone for 24 hr. The cells were removed from the dish with a rubber policeman, a procedure that left the vast majority of the cells intact. The cell suspension was stored at room temperature and used within 12 hr for all the experiments reported here. However, 24 hr of incubation at room temperature did not yield significantly different results. Trypsin treatment of the cells before use was avoided, because the HK2 channel has six potential tryptic cleavage sites on its presumed extracellular face (11).

Electrical recording. Micropipettes were pulled from Radnoti borosilicate glass and were heat polished. They were filled with "intracellular" solution (see below) and connected to the headstage of an Axopatch-1A patch-clamp amplifier. All currents were recorded at room temperature. The current records were sampled at 3–10 times the anti-alias filter setting, stored on the hard disk of an IBM-PCAT for subsequent analysis, and archived on optical disk. Data acquisition and command potentials were controlled by a versatile custom-made programmable stimulator. Gain, filter frequency, and temperature were stored with each record. To ensure voltage-clamp quality, microelectrode resistance was kept below 3.5 MΩ; average resistance was 2.0 ± 0.6 MΩ (n = 14). The microelectrodes were gently lowered onto the cells, and gigaohm seal formation (16 ± 9 GΩ; range, 6–33 GΩ) was achieved by suction. After seal formation, cells were lifted from the bottom of the perfusion bath and the membrane patch was ruptured with brief additional suction. The capacitive transients elicited by symmetrical 10-mV steps from −80 mV were recorded at 50 kHz (filtered at 10–20 kHz) for subsequent calculation of capacitive surface area, access resistance, and input impedance. Resting potential was recorded in current-clamp mode and checked intermittently throughout the experiment. Thereafter, capacitance and series resistance compensation were optimized, and 80% compensation was usually obtained. With an average current of 2.5 nA at +50 mV, no significant voltage errors due to series resistance are expected with the electrodes used, and this was confirmed by the calculated R_s. The low capacitance (19 ± 2 pF) enabled fast clamp control ($\tau \sim 100$ μsec before compensation and $\tau \sim 40$ μsec after compensation).

Solutions. The intracellular pipette filling solution contained (in mM) 110 KCl, 10 HEPES, 5 K_4BAPTA, 5 K_2ATP, and 1 $MgCl_2$, and was adjusted to pH 7.2 with KOH, yielding a final intracellular K^+ concentration of 145 mM. The bath solution contained (in mM) 130 NaCl, 4 KCl, 1.8 $CaCl_2$, 1 $MgCl_2$, 10 HEPES, and 10 glucose and was adjusted to pH 7.35 with NaOH. To obtain higher extracellular K^+ concentrations, equimolar substitution of KCl for NaCl was used. Quinidine was added from a stock solution of 10 mM (quinidine gluconate; Eli Lilly, Indianapolis, IN).

Pulse protocols and analysis. After control data were obtained, bath perfusion was switched to drug-containing solution. Drug infusion or removal was monitored with test pulses from −80 mV to +50 mV, applied every 30 sec until steady state was obtained (within 10–15 min).

The holding potential was −80 mV unless indicated otherwise. In drug-free conditions, repriming kinetics of HK2 (deactivation and recovery from slow inactivation) were sufficiently fast to allow for pulse trains at 0.5 Hz without decrement of the current. In the presence of 20 μM quinidine, a pulse frequency of 0.1 Hz could be used without "use-dependent" accumulation of block (with 250-msec depolarizations). Therefore, the cycle time for any protocol was 0.1 Hz or slower (with the exception of specific pulse trains).

The protocol to obtain current-voltage (I-V) relationships and activation curves consisted of 250-msec pulses that were imposed in 10-mV increments between −80 and +60 mV, with additional interpolated pulses to yield 5-mV increments between −30 and +10 mV (activation range of HK2). The "steady state" I-V relationships were obtained by measuring the current at the end of the 250-msec depolarizations. Between −80 and −40 mV, only passive linear leak was observed; least squares fits to these data were used for passive leak correction. Deactivating 'tail' currents were recorded at −30 or −50 mV. The activation curve was obtained from the tail current amplitude immediately after the capacitive transient or from the amplitude of the exponential fit to its time course. Both gave similar results in controls. All measurements were done by a custom-made analysis program that recognized the protocol identifier and applied the appropriate analysis procedure for each protocol to extract I-V relationships, peak currents, activation curve etc. For steady state curves, raw data points were averaged over a small time window (2–5 msec). Peak currents were obtained from the best second-order polynomial fit to the raw data points, using a moving window of 10–20 msec, as used previously for analyzing I_{Na} (6). Raw tracings shown in this paper are leak subtracted, as described above, and digitally filtered at 1 kHz in the frequency domain after Fourier transformation.

Activation curves were fitted with a Boltzmann equation

$$y = \frac{1}{1 + e^{-s \cdot (E - E_h)}} \quad (1)$$

in which s represents the slope factor and E_h the voltage of 50% activation (or inactivation). The time course of tail currents and slow inactivation were fitted with a sum of exponentials, and activation kinetics were fitted to an equation of the form $(1 - A \times \exp(-t/\tau_n))^n$, with $n = 4$ (19, 20). The curve-fitting procedure used a nonlinear least-squares (Gauss-Newton) algorithm; results were displayed in linear and semilogarithmic format, together with the difference plot. Goodness of the fit was judged by the χ^2 criterion and by inspection for systematic nonrandom trends in the difference plot.

A first-order blocking scheme was used to describe drug-channel interaction (see Discussion); apparent affinity constant, K_D, and Hill coefficient, n_H, were obtained from fitting of the fractional block, f, at various drug concentrations, $[D]$, to:

$$f = \frac{1}{1 + (K_D/[D])^{n_H}} \quad (2)$$

and apparent rate constants for binding (k) and unbinding (l) were obtained from solving:

$$k \cdot [D] + l = \lambda (= 1/\tau_B) \quad (3a)$$

$$\frac{l}{k} = K_D \quad (3b)$$

in which λ is the inverse of the time constant of block development, τ_B. The validity of this approach is addressed in the Discussion.

Voltage dependence of block was determined as follows: leak-corrected current in the presence of drug was normalized to matching control, to yield fractional block at each voltage ($f = 1 - I_{quinidine}/I_{control}$). The voltage dependence of block was fitted to

$$f = \frac{[D]}{[D] + K_D^* \cdot e^{-\delta z F E / RT}} \quad (4)$$

where z, F, R, and T have their usual meaning and δ represents the fractional electrical distance, i.e., the fraction of the transmembrane electrical field sensed by a single charge at the receptor site. K_D^* represents the affinity at the reference voltage (0 mV).

Statistical methods. Results are expressed as mean ± standard deviation. ANOVA was used to compare the effect of quinidine with control; $p < 0.05$ was considered significant.

Results

Dose-dependent and reversible block. Fig. 1 shows recordings of potassium current through HK2 channels expressed in mouse L cells. Under control conditions (Fig. 1A), the HK2 current rose rapidly, with a sigmoidal time course, to a peak and then declined slowly (slow and partial inactivation). Outward tail currents were observed upon repolarization to −50 mV. Activation time constants ranged from 40 msec at −20 mV to 2 msec at +60 mV.

Fig. 1, B, C, and D, shows the effect of sequential application of 6, 20, and 60 μM quinidine, respectively. Quinidine reduced the outward potassium current in a dose-dependent manner, and this effect was reversible. Fig. 1E shows that the current was restored to 85% of control in 20 min after return to control solution. Induction of block after switching of perfusion progressed with a time constant of 3–4 min, which was about 5 times slower than the effect of changing extracellular K^+ concentration at similar flow rates. This suggested an intramembrane or intracellular site of action and, therefore, 20 min of equilibration were allowed before assessment of drug effects. Quinidine not only reduced the current but also altered the time course of the current during depolarization. The potassium

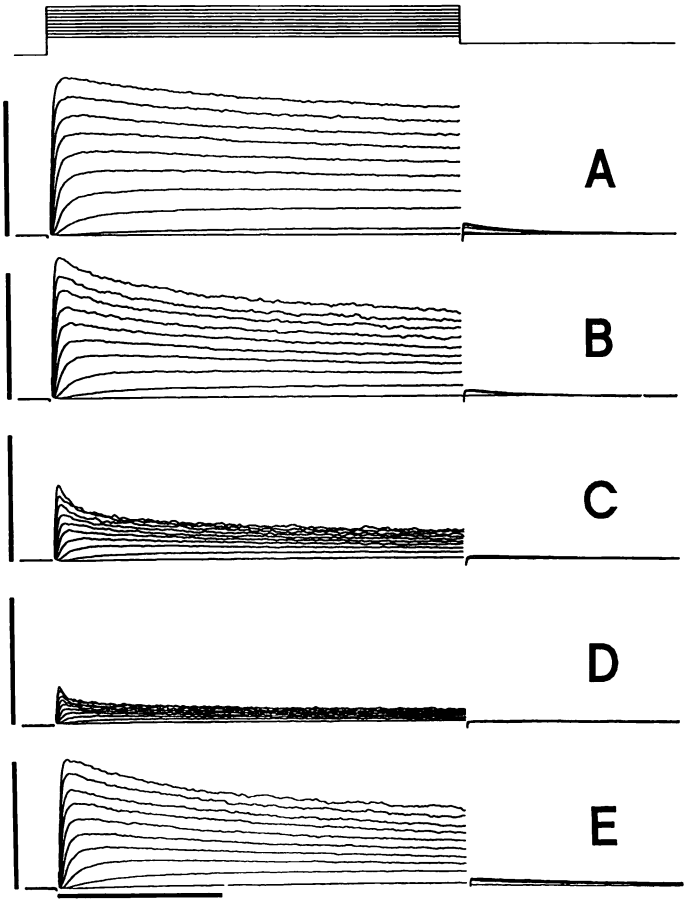

Fig. 1. Reduction of HK2 current by quinidine. Currents are shown for depolarizations from −80 mV to voltages between −30 and +60 mV in steps of 10 mV; tail currents were obtained at −50 mV. A–E, control, 6 μM, 20 μM, and 60 μM quinidine, and wash out (20 min), respectively. After addition of quinidine, the current at the end of the depolarization (250-msec I-V) was reduced in a dose-dependent manner at all voltages. The effects were largely reversed after 20 min of wash out. Cell capacitance, 20 pF. *Vertical calibration*, 2 nA (=100 pA/pF); *horizontal bar*, 100 msec. Data filtered at 2 kHz (four-pole Bessel) and digitized at 10 kHz; digital leak subtraction and additional digital filtering at 1 kHz.

current initially activated as in control but subsequently declined markedly. This decline occurred much more quickly and to a greater extent than the slow inactivation observed in control. Analysis of this time course of block (see below, Fig. 5) indicated that a steady level is achieved within 250 msec, whereas slow inactivation was limited over this time. Therefore, the reduction of the HK2 current at the end of a 250-msec depolarization was used as an index of block ($f = 1 - I_{quinidine}/I_{control}$). In the experiment shown in Fig. 1, the K^+ current at +50 mV was reduced to 68%, 29%, and 5% of control after application of 6, 20, and 60 μM quinidine, respectively.

Fig. 2 shows pooled data from 12 experiments for the concentration dependence of block observed during depolarization to +60 mV. Block averaged 28 ± 6% ($n = 2$) at 2 μM, 48 ± 15% ($n = 3$) at 6 μM, 72 ± 6% ($n = 8$) at 20 μM, and 91 ± 3% ($n = 4$) at 60 μM. A nonlinear least-squares fit of the concentration-response equation (eq. 2) (see Materials and Methods) to the individual data points yielded an apparent K_D of 6.24 μM and a Hill coefficient of 0.89. This fit is represented by the solid line in Fig. 2. The dashed line illustrates a fit to the same data with the Hill coefficient fixed at 1; the apparent K_D was similar.

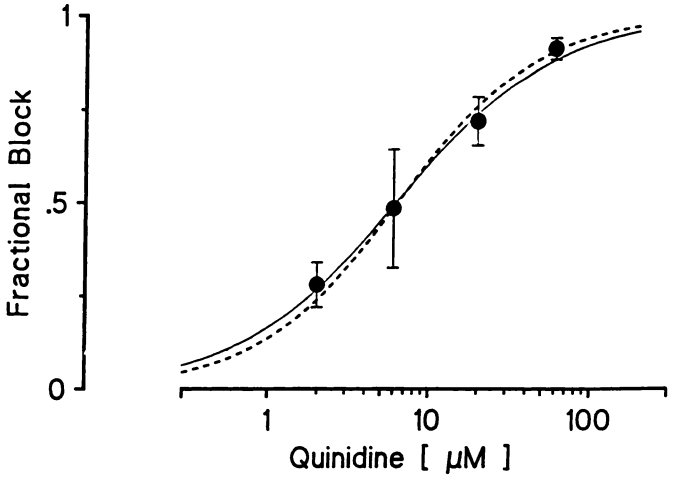

Fig. 2. Concentration dependence of quinidine-induced block of HK2. Reduction of current (relative to control) at the end of depolarizations to +60 mV was used as index of block. Data are mean ± standard deviation from a total of 14 experiments. ——, Fit with equation $1/(1 + (K_D/[D])^{n_H})$; – – –, for comparison, the fit for a Hill coefficient of 1.

This Hill coefficient close to unity suggests that binding of one quinidine molecule/channel is sufficient to block potassium permeation.

Voltage-dependent block. Fig. 3A shows the effect of 20 μM quinidine on the steady state current-voltage (I-V) relationship for this K^+ channel. The I-V relationship in control was almost linear for depolarizations positive to +10 mV; the sigmoidicity between −30 and +10 mV reflected the voltage dependence of channel gating. In the presence of quinidine, the curve displayed a moderate downward curvature positive to 0 mV. This is indicative of more extensive block at the larger depolarizations. To quantitate this voltage dependence, the relative current $I_{quinidine}/I_{control}$ was plotted as a function of voltage (Fig. 3B). Block increased steeply between −30 mV and 0 mV, coinciding with the voltage range of channel opening shown by the dashed line in Fig. 3B. These data suggest that quinidine binds primarily to the open state. Between 0 mV and 60 mV, block continued to increase with a more shallow voltage dependence, despite the fact that all channels are open over this voltage range. With 20 μM, block increased from 0.60 ± 0.09 at 0 mV to 0.72 ± 0.06 at +60 mV ($n = 8$), and with 6 μM from 0.39 ± 0.20 at 0 mV to 0.48 ± 0.16 at +60 mV ($n = 3$). ANOVA of the results with 20 μM quinidine indicated that the increase in block between 0 and +60 mV was statistically significant (ANOVA, $p = 0.03$ with values for 0, +30, and +60 mV); a paired comparison between block at 0 mV and +60 mV yielded $p < 0.001$.

It is unlikely that this shallow voltage dependence was due to channel gating, because HK2 activation had reached saturation over this voltage range (Fig. 3B), with time constants of 10 msec or less. Quinidine is a base and has a tertiary amine group with $pK_a = 8.9$. At the intracellular pH of 7.2, quinidine is, therefore, present predominantly in the charged form. The voltage dependence of block could, therefore, be due to the effect of the transmembrane electrical field on the interaction between the quinidine ion and the channel receptor; if quinidine reaches the receptor from the inside, then channel block is expected to increase in a voltage-dependent manner, according to the Boltzmann relationship, $[D]/([D] + K_D^0 \times \exp(-z\delta FE/RT))$ (eq. 4 in Materials and Methods). The parameter δ in this equation represents the fractional electrical distance, i.e., the fraction of the membrane electrical field sensed by a single charge, at the receptor site. The solid line in Fig. 3B represents the fit of this equation to the data points positive to 0 mV (solid symbols), with a fractional electrical distance $\delta = 0.18$ for this experiment. In seven experiments with 20 μM quinidine, the average value for δ was 0.19 ± 0.02.

The voltage dependence of block was similarly obtained in experiments with 2, 6, and 60 μM quinidine. The average value for block at 0 mV, +30 mV, and +60 mV at each concentration is shown in Fig. 4. The solid line for 20 μM quinidine was calculated from eq. 4 with $\delta = 0.19$ and apparent $K_D = 6.24$ μM (from Fig. 2). This equation predicts the voltage dependence for the other concentrations without additional free parameters. The solid lines in Fig. 4 indicate that the predicted voltage dependence corresponded very well to the experimental results obtained for 2, 6, and 60 μM quinidine.

Concentration dependence of time course of channel block. If quinidine can only access its receptor if the channel is in the open state, then inhibition of the potassium current would only develop as channels start to open, and block development should be visible if the blocking rate is slower than the opening rate. If the blocking rates were faster, or if quinidine blocked other states, the current would be expected to be simply scaled down. Fig. 5 shows a superposition of the tracings obtained at +60 mV in control and with 6, 20, and 60 μM quinidine. In control, the K^+ current reached its peak at 10

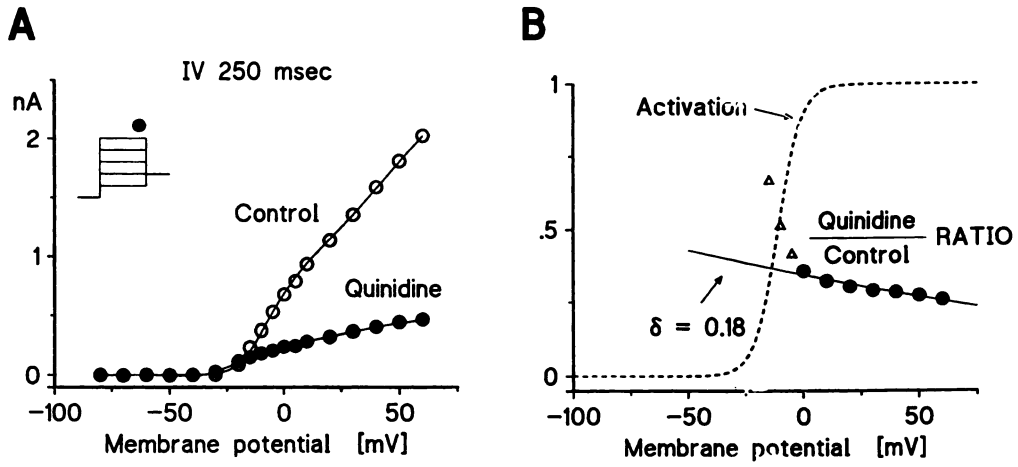

Fig. 3. Voltage dependence of HK2 block by quinidine (20 μM). A, Current-voltage relation (250 msec isochronal) in control and with drug. B, Relative current ($I_{quinidine}/I_{control}$) from data in A. – – –, Activation curve for this experiment. Block increased steeply between −20 mV and 0 mV (△), the voltage range of activation of HK2. Positive to 0 mV, a continued but more shallow voltage dependence was observed (●). This voltage dependence was fitted with eq. 4 (see Materials and Methods) and yielded $\delta = 0.18$ (——).

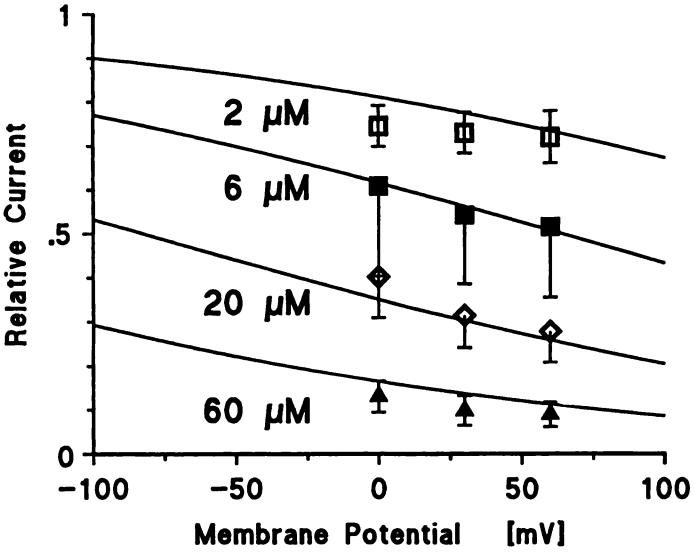

Fig. 4. Voltage and concentration dependence of HK2 block. The relative current obtained at 0, +30, and +60 mV id displayed as mean ± standard deviation for the indicated concentrations. Paired analysis indicated that the voltage dependence of block was significant (see text). The *solid line* for 20 μM was calculated from eq. 4, with following parameters: $\delta = 0.19$ (obtained from seven experiments with 20 μM) and $K_D = 6.2$ μM (from Fig. 2). The *solid lines* for the other concentrations are the predictions from eq. 4, with these values for δ and K_D (i.e., no free parameters).

msec and then declined slowly, with a time constant of 156 msec. In the presence of quinidine the peak was smaller and was reached at earlier times. The subsequent time course displayed an additional exponential component superimposed on the slow inactivation. The time constants of the fast component were 14, 8, and 4 msec for 6, 20, and 60 μM quinidine, respectively. This extra component was at least 10 times faster than the slow inactivation for quinidine concentrations of 6–60 μM. Therefore, this time constant (τ_{block}) was considered to be a reasonable approximation of the drug-channel interaction kinetics (see Discussion). Fig. 5B shows the plot of $1/\tau_{block}$ versus drug concentration for data obtained from four experiments; the straight line is the least squares fit to the relation $1/\tau_B = k \times [D] + l$. Slope and intercept for the fitted relation yielded an apparent association rate $k = 4.5 \times 10^6$ M^{-1} sec^{-1} and dissociation rate $l = 34$ sec^{-1}. This yielded an apparent $K_D = l/k = 7.5$ μM for these experiments, in close agreement with the value of 6.2 μM (all experiments).

In 20 μM quinidine, the fast time constant averaged 8.4 ± 1.1, 8.1 ± 2.2, and 8.2 ± 0.8 msec at +40 mV, +50 mV, and +60 mV, respectively ($n = 8$). The differences among these values were not statistically significant. In the presence of quinidine, the slow time constant was slightly faster than in control, but the difference was either not significant or barely significant ($0.04 < p < 0.25$ at voltages between +30 and +60 mV).

Time course of tail currents. At −50 mV, the potassium current deactivated completely, with a time constant of approximately 40 msec. This time constant reflects mainly the virtually irreversible closing of the channel. If quinidine only blocks the open channel, then dissociation of quinidine from the blocked channel results in an open channel (which subsequently could close). Blocked channels are not conducting, and the conversion to open channels should, therefore, result initially in a rising phase of the tail current; subsequently, the tail current should display a slower decline because some fraction of the open channels become blocked again, rather than closing irreversibly. Fig. 6 shows the superposition of the tail currents obtained at −50 mV after a 250-msec depolarization to +50 mV under control conditions and in the presence of 6 and 20 μM quinidine (results from two different experiments are shown). In control, the tail declined with a time constant of 35 msec (Fig. 6A) and 51 msec (Fig. 6B). After exposure to quinidine, the amplitude was reduced and the time course altered. In 20 μM the tail current displayed a definite rising phase, reaching a peak after 29 msec; in 6 μM the effect was similar but less pronounced. The subsequent decline of the tail current was slower than in control ($\tau = 52$ and 177 msec for 6 and 20 μM quinidine, respectively), resulting in the "crossover" phenomenon in both panels of Fig. 6. Similar results were obtained in the other experiments.

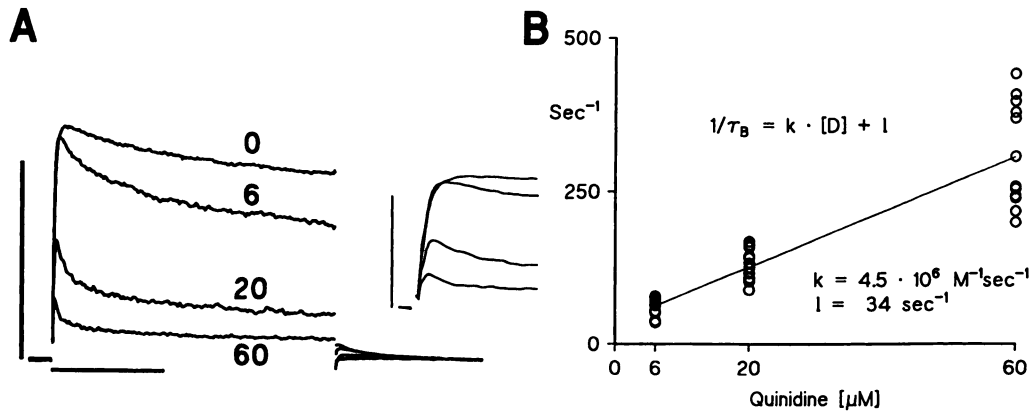

Fig. 5. Kinetics of block induction. A, Superimposed tracings for steps from −80 mV to +50 mV are shown for control and 6, 20, and 60 μM quinidine. In the presence of quinidine, the current activated initially as in control (*inset*) but reached a lower peak and subsequently declined more quickly. *Calibration*: *horizontal*, 100 msec; *vertical*, 2 nA. *Inset*, first 25 msec. B, Rate of block as function of concentration. The time constant of the quinidine-induced fast component (τ_B) was obtained from biexponential fits to the falling phase of the tracings in A. The inverse of τ_B is plotted versus concentration. For a first-order blocking scheme, a linear relation is expected: $1/\tau_B = k \times [D] + l$. The *solid line* epresents the linear fit, from which the apparent binding and unbinding rate constants were obtained.

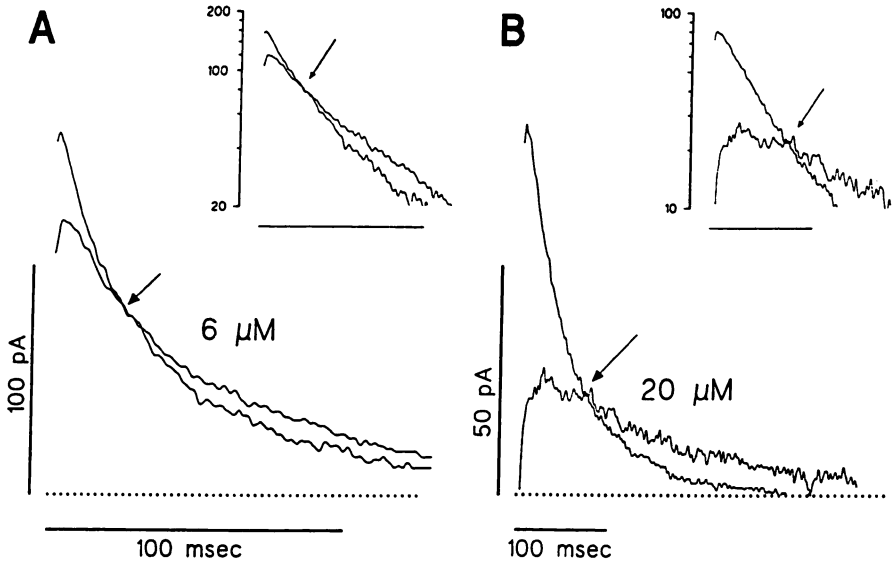

Fig. 6. Tail current crossover. A, 6 μM quinidine; B, 20 μM quinidine. Tail currents were obtained at −50 mV, after a 250-msec depolarization to +50 mV. *Calibrations*: *horizontal*, 100 msec; *vertical*, 100 pA (A) and 50 pA (B). *Inset*, same tails in semilogarithmic format. The tail current in control is the largest tracing, which deactivated the most quickly. *Arrow*, crossover of tracing in quinidine with the control tracing.

Discussion

This investigation into the mechanism of quinidine block of the HK2 potassium channel is the first pharmacological study of a human cardiac K^+ channel expressed in permanently transfected mammalian tissue culture cells. Under the experimental conditions used in this study, voltage-gated K^+ currents were only observed in the HK2-transfected mouse L cells. This tissue culture system has several advantages over the commonly used oocyte expression system; 1) a clonal cell line ensures reproducible results and avoids problems with variability in oocyte quality and 2) the L cells are mammalian cells and their plasma membrane, therefore, more closely resembles that of the cardiac myocyte.

Quinidine produces time-dependent block of the open HK2 channel. The antiarrhythmic agent quinidine displayed state-, time-, and voltage-dependent interactions with this human cardiac potassium channel. The data presented in this paper indicate that quinidine binds to the open state of the channel because 1) the initial time course of activation was not modified (Fig. 5), 2) block mainly occurred after channel opening (Figs. 1 and 5), and 3) block increased sharply in the voltage range of channel activation (Fig. 3B). Therefore, we will interpret the results with reference to the following kinetic state diagram for the channel:

$$\begin{array}{ccccccccc} & 4\alpha & 3\alpha & 2\alpha & \alpha & k\cdot[D] & & \\ \mathrm{C} & \rightleftharpoons & \mathrm{C} & \rightleftharpoons & \mathrm{C} & \rightleftharpoons & \mathrm{O} & \rightleftharpoons & \mathrm{OB} \\ & \beta & 2\beta & 3\beta & 4\beta & & l & & \\ & & & & \updownarrow & & & & \\ & & & & \mathrm{I} & & & & \end{array}$$

Scheme A

This scheme is similar to those used for the related *Shaker* and RCK1 channels (19, 20). Upon depolarization, the channel opens rapidly (C→C→C→C→O) and then slowly inactivates (O→I). Channel opening was fast ($\tau_n \sim 2$ msec at +50 mV). A component of partial slow inactivation could be resolved on the time scale of the tracings shown in this report; the time constant was around 150 msec.

A simple way to incorporate the interaction of quinidine into the state diagram is to assume that quinidine binds to the open state of the channel, as indicated in scheme A. Because activation is fast, positive to 0 mV, this system functionally reduces to a three-pool model (I⇌O⇌OB). In the presence of quinidine, the 'inactivation' became biexponential, as expected for this model. The quinidine-induced extra component of inactivation had a time constant that was much faster than that of slow inactivation; therefore, this fast time constant can be considered to represent the interaction of quinidine with the open state (O⇌OB), $\tau_B = 1/(k \times [D] + l)$.

We recognize that the assumption that the fast component represents the O⇌OB transition does not hold at small depolarizations (below 0 mV), where activation is much slower, or at low drug concentrations, in which case the time constant of block may be similar to that of inactivation. In these cases scheme A is still valid, but extraction of the binding and unbinding rates is more complex (it requires the full analytical solution of the three-pool model). Therefore, data on 2 μM quinidine were not incorporated in Fig. 5.

Based on this model, the apparent binding and dissociation rates for quinidine were calculated to be $k = 4.5 \times 10^{+6}$ sec^{-1} M^{-1} and $l = 34$ sec^{-1}, respectively (Fig. 5). The binding rates can also be derived from the apparent K_D (6.2 μM), and the average value of the time constant of block in 20 μM quinidine (8.1 msec). This yielded $k = 4.7 \times 10^{+6}$ sec^{-1} M^{-1} and $l = 29$ sec^{-1}, i.e., both methods yield similar values.

Open-channel block not only affects the time course of the current during depolarization but also can modify the tail current. Upon repolarization, channel deactivation is fast and virtually irreversible ($4\beta \gg \alpha$). If a large fraction of the channels are blocked (OB) and the unbinding rate l is fast enough, then the tail may display a rising phase reflecting the OB→O unblocking. Subsequently, the tail should deactivate more slowly than in control, because a fraction of the unblocked channels become blocked again; the latter depends on the relative values of $k \times [D]$ and 4β. Therefore, this model predicts for the tail currents, in the presence of quinidine, 1) an initial rising phase and 2) a slower deactivation. Fig. 6 shows that a rising phase was prominent with 20 μM quinidine (tail reached peak around 25 msec), but less so with 6 μM. With both concentrations, the crossover is obvious. Therefore, the results for the tail currents provide additional support for the proposed open-state block mechanism of quinidine.

Fig. 7 shows the result of a mathematical simulation of the

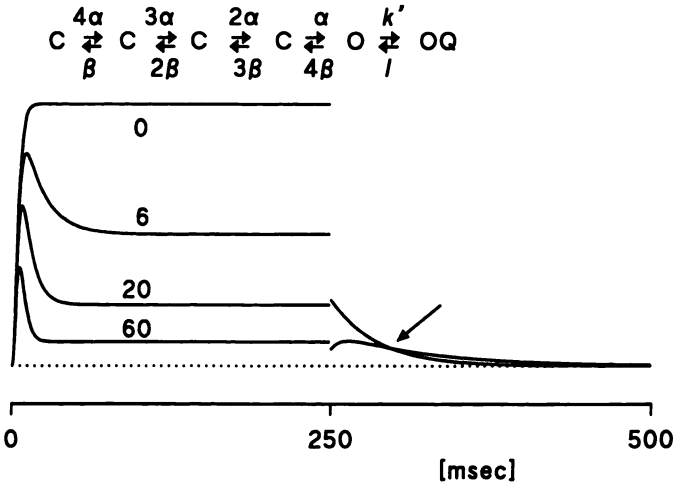

Fig. 7. Model simulation of quinidine-HK2 interaction. The open-channel block model (scheme A) was used with the following rate constants: at +50 mV, $\alpha = 400$ sec^{-1}, $\beta = 1$ sec^{-1}, $k = 5$ μM^{-1} sec^{-1}, and $l = 30$ sec^{-1}; at −50 mV, $\alpha = 0.1$ sec^{-1}, $\beta = 7$ sec^{-1}, $k = 2.75$ μM^{-1} sec^{-1}, and $l = 55$ sec^{-1}. For depolarization, simulations for control and for 6, 20, and 60 μM quinidine are displayed; for the tails, control and 20 μM quinidine are shown. *Arrow*, crossover. Currents for step and tail were scaled to reflect the difference in driving force. Simulations were done using a standard Runge-Kutta method with variable step size.

effects of 20 μM quinidine, based on this open-channel block model (scheme A). The voltage dependence of the drug-channel interaction was incorporated, but inactivation was omitted for simplicity. Activation was modeled with four independent gating units (corresponding to the tetramer structure of the channel) (see also Refs. 19–21), with rate constants reproducing activation and tail kinetics in control. Incorporation of the experimentally obtained values for k and l rate constants reproduced the experimental observations of both block induction and tail current morphology. Both in the experimental recordings (Fig. 5) and in the model, the peak current is suppressed about 50% at 20 μM. In the model, this is due solely to the open-channel interaction and is not attributable to preexisting block, because the simulation started with all channels in the drug-free rested state and incorporated only open-channel block. Thus, the major features of the block of HK2 by quinidine may be explained by the open-channel block model, with a voltage-dependent component due to the ammonium ion behavior of quinidine at physiological pH. This model is similar to the model originally proposed by Armstrong (22) for the interaction of quaternary ammonium derivatives with neuronal K^+ channels.

Open-channel block is voltage dependent. Drugs that interact predominantly with the open state of the channel can do so by moving into the ion-conducting pore. If a positively charged drug moves into the membrane electrical field from the inside, then block should increase upon depolarization (according to eq. 4). This should happen even over the voltage range where all channels are open. With a pK_a of 8.9, quinidine is predominantly charged at physiological pH. Figs. 3 and 4 show that HK2 block by quinidine was indeed voltage dependent. The $\delta = 0.19$ value for the voltage dependence of the apparent K_D, can, therefore, be interpreted to indicate that quinidine moves about 20% into the membrane electrical field to reach the receptor and block ion current (or, more precisely, that the positively charged amine senses that fraction of the electrical field). An alternative explanation for the voltage dependence of quinidine block could be that the drug binding site is allosterically linked to the channel voltage-sensing apparatus and that, due to some property of the receptor, k and l would change as a function of voltage. This explanation is unlikely for two reasons. First, the observed voltage dependence of block was measured over a voltage range where the channels are maximally activated. Second, the magnitude of the voltage dependence is similar to that measured for TEA, a compound likely to bind in the ion pore (16).

The voltage dependence of the apparent K_D, implies that k and/or l are voltage dependent ($k = k_0 \times e^{+\delta zFE/2RT}$, $l = l_0 \times e^{-\delta zFE/2RT}$). Therefore the time constant for block (τ_B) should also be voltage dependent. However, with the value $\delta = 0.19$, the calculated voltage dependence of τ_B is shallow and results in a <1-msec difference over the voltage range +30 to +60 mV. This would be difficult to detect, and most likely explains why experimentally we did not observe significant differences in τ_B between +40 and +60 mV.

Does quinidine block closed channels? The applicability of model A does not disprove the possibility of closed-channel block. The reduction of the maximum peak current attained during depolarization in the presence of quinidine could be considered a measure of rested-state block. However, block observed at the time of the peak includes 1) rested-state block, 2) true open-state block developed before the time of the peak (Fig. 7), and 3) block of intermediate activated, but nonconducting, states (23).

It has been argued that internal TEA block of squid K^+ channels is independent of channel state (24). The state diagram for such interaction is shown as scheme B (in schemes B and C, $k' = k \times [D]$). If quinidine blocks the HK2 channel in this manner, irrespective of channel state, then true rested-state block is expected. With the voltage dependence of quinidine action, block at −80 mV is expected to be less than at +50 mV but still substantial. The observed voltage dependence of the apparent K_D predicts approximately 50% block at −80 mV for 20 μM quinidine (see Fig. 4). Compared with the open-channel block model (scheme A), this would result in 1) a similar steady state level of block at depolarized potentials but 2) a much larger depression of the initial current than observed in the experimental records and 3) no component of block coinciding with channel activation (open symbols in Fig. 3). In addition, this model allows relief of block bypassing the open state, i.e., it does not produce tail crossover (24). Based on the results available for HK2, this state-independent block model is unlikely unless the affinity for the rested state differs more than expected from the voltage dependence. (If a much lower rested-state affinity is assigned, then the model is no longer state independent but becomes a general modulated receptor model.)

$$\begin{array}{ccccccccc} & 4\alpha & & 3\alpha & & 2\alpha & & \alpha & \\ C & \rightleftharpoons & C & \rightleftharpoons & C & \rightleftharpoons & C & \rightleftharpoons & O \\ & \beta & & 2\beta & & 3\beta & & 4\beta & \\ l \downuparrows k' & & l \downuparrows k' & & l \downuparrows k' & & l \downuparrows k' & & l \downuparrows k' \end{array} \qquad \text{Scheme B}$$

$$\begin{array}{ccccccccc} & 4\alpha & & 3\alpha & & 2\beta & & a & \\ B & \rightleftharpoons & B & \rightleftharpoons & B & \rightleftharpoons & B & \rightleftharpoons & B \\ & \beta & & 2\beta & & 3\beta & & 4\beta & \end{array}$$

$$\begin{array}{ccccccc} 4\alpha & & 3\alpha & & 2\alpha & & \alpha \\ D_4 & \rightleftharpoons & D_3A_1 & \rightleftharpoons & D_2A_2 & \rightleftharpoons & D_1A_3 \rightleftharpoons A_4 \\ \beta & & 2\beta & & 3\beta & & 4\beta \\ l \downuparrows k' & & l \downuparrows 2k' & & l \downuparrows 3k' & & l \downuparrows 4k' \end{array} \qquad \text{Scheme C}$$

$$\begin{array}{ccccc} & 3\alpha & & 2\beta & \\ D_3B & \rightleftharpoons & D_2A_1B & \rightleftharpoons & D_1A_2B \rightleftharpoons A_3B \\ & \beta & & 2\beta & 3\beta \end{array}$$

An intermediate model, which deserves consideration in light of the four-fold symmetry of the channel (21), is shown as scheme C. Here it is assumed that each of the four subunits contains a separate receptor. This receptor is available for interaction with quinidine when the subunit is activated (A) and, if any of the subunits bind quinidine, ion permeation is prevented. In this model, true rested-state (D_4) block does not exist, but block of the intermediate partially activated channel ($D_3A_1 - D_1A_3$) occurs, in addition to block of the open state ($A_4 \rightleftharpoons A_3B$). The time course of block in this model depends on the exact kinetic model of channel gating but qualitatively resembles the open-channel block model for block induction. The steady state block level is similar to that of the open-state model (scheme A), but the initial depression of the peak current is higher at high drug concentrations (but not as extensive as in scheme B). However, scheme C can produce recovery from block without channel opening and does not necessarily result in a crossover. More detailed experiments focusing on the recovery kinetics and block development at intermediate potentials are needed to determine the possible contribution of partially activated-state block. An extension of this model would be to allow up to four quinidine molecules to bind to the channel (one per subunit). This would produce even more pronounced differences in recovery from block between schemes A and C.

Structural implications for receptor topology. A first implication from this study is that the binding site for quinidine appears to be located on the channel itself and not on some associated subunit. Only the HK2 channel coding sequence was transfected; therefore, any subunit that could be associated with the channel in native cells is absent in the expression system (unless the fibroblasts happen to have an appropriate subunit).

The observed voltage dependence of block strongly suggests that the binding site is within the transmembrane electrical field. Therefore, the interaction of quinidine is expected to occur on membrane-spanning or intramembrane segments of the channel. HK2 displays a high degree of homology with *Drosophila Shaker* (*Sh*), especially in the transmembrane segments (95% identity in segments S4–S6). In the *Shaker* K^+ channels, the ion-conducting pore has recently been localized to amino acids 431–449 (16, 25, 26). The amino acid sequence 462–480 of HK2 (Fig. 8) is identical to this "pore" sequence of *Shaker*, with the exception of the last amino acid (arginine in HK2, threonine in *Shaker*). Mutations on either end of the ion pore in *Shaker* alter the affinity for TEA (T441S for internal and T449Y for external TEA). Interestingly, internal TEA block of *ShB* has a voltage dependence described by a fractional electrical distance of 0.15 (16). This suggests that internal TEA moves about 15% into the transmembrane electrical field. The T441S mutation reduces affinity for internal TEA and is, therefore, assumed to be located near or at the TEA binding site 15% into the electrical field. The functional similarity between quinidine block of this human cardiac K^+ channel and the quaternary ammonium block of the *Shaker* channels and the high structural similarity of the ion pores suggest that the T472 residue (equivalent of T441 *Sh*) in HK2 may be involved in quinidine binding. The hypothesis that T472 is involved in quinidine block will be tested directly using point mutations.

Although mutations of the neighboring pore amino acids of *ShB* did not alter internal TEA sensitivity (16), these residues

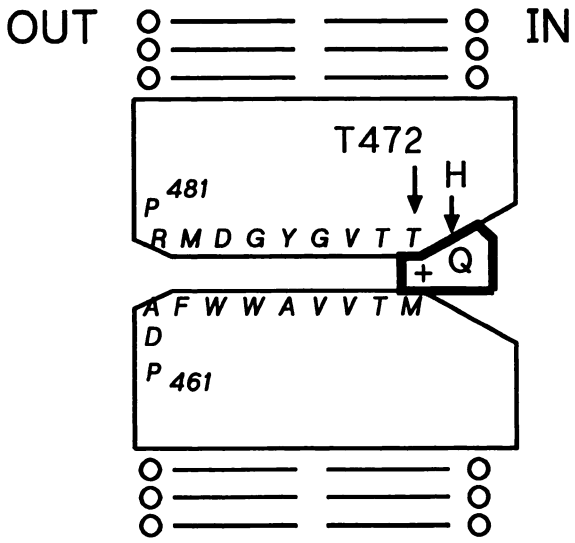

Fig. 8. Possible binding site for quinidine in the HK2 pore. One subunit is shown, with the putative pore-lining amino acid sequence superimposed. The internal threonine residue (*arrow* at T472) involved in TEA block (in *Shaker* K^+ channels) is shown about 20% into the bilayer. *Q*, quinidine; +, its charged amine function. The drug is shown occluding the inner pore mouth; *arrow* (*H*) *above Q*, additional hydrophobic binding to other adjacent parts of the HK2 channel. Four of these subunits are assumed to form the functional HK2 channel.

may be involved in binding the hydrophobic domains of quinidine ($\log P = 2.4$) (23) and thus may be responsible for the enhanced affinity of quinidine, relative to TEA. The apparent affinity of the HK2 channel for quinidine is ~6 μM at +60 mV or ~9 μM at 0 mV, whereas the affinity of *ShB* for internal TEA is 700 μM (16). Various K^+ channels tend to have a higher affinity for quaternary ammonium compounds with longer alkyl side chains or aromatic rings (for review, see Ref. 27). For example, the affinity of squid K^+ channels for tetrapentyl ammonium is 10-fold higher than that for TEA. The increase in affinity with more hydrophobic side chains indicates that binding of these agents is stabilized by hydrophobic interactions. In preliminary experiments, we have also observed that the affinity of HK2 for tetrapentyl ammonium and for the class III agent clofilium is below 1 μM. The micromolar affinity of HK2 for quinidine thus suggests that the receptor consists of an area for electrostatic interactions and one or more domains for hydrophobic interactions (Fig. 8).

Acknowledgments

We thank Dr. Paul Bennett for helpful discussions during this study and Drs. Albert Beth, Dan Roden, and David Lovinger for critical review of the manuscript. We thank Craig Short for technical assistance.

NOTE ADDED IN PROOF

Under the recently proposed nomenclature for cloned K^+ channels (Chandy, K. G. Simplified gene nomenclature. *Nature (Lond.)* **352:** 26, 1991 (scientific correspondence)), the HK2 and RK4 channels would be classified as human cardiac Kv1.5 and rat cardiac Kv1.5, respectively (based on 86% homology between both).

References

1. Salata, J. J., and J. A. Wasserstrom. Effects of quinidine on action potentials and ionic currents in isolated canine ventricular myocytes. *Circ. Res.* **62:**324–337 (1988).
2. Weld, F. M., J. Coromilas, J. N. Rottman, and J. T. Bigger. Mechanisms of quinidine-induced depression of maximum upstroke velocity in ovine cardiac Purkinje fibers. *Circ. Res.* **50:**369–376 (1982).
3. Imaizumi, Y., and W. R. Giles. Quinidine-induced inhibition of transient outward current in cardiac muscle. *Am. J. Physiol.* **253:**H704–H708 (1987).
4. Packer, D. L., A. O. Grant, H. C. Strauss, and C. F. Starmer. Characterization of concentration- and use-dependent effects of quinidine from conduction

delay and declining conduction velocity in canine Purkinje fibers. *J. Clin. Invest.* **83**:2109–2119 (1989).
5. Hondeghem, L. M., and B. G. Katzung. Test of a model of antiarrhythmic drug action: effects of quinidine and lidocaine on myocardial conduction. *Circulation* **61**:1217–1224 (1980).
6. Snyders, D. J., and L. M. Hondeghem. Effects of quinidine on the sodium current of ventricular guinea-pig myocytes: evidence for a drug-associated rested state with altered kinetics. *Circ. Res.* **66**:565–579 (1990).
7. Furukawa, T., Y. Tsujimura, K. Kitamura, H. Tanaka, and Y. Habuchi. Time- and voltage-dependent block, of the delayed K^+ current by quinidine in rabbit sinoatrial and atrioventricular nodes. *J. Pharmacol. Exp. Ther.* **251**:756–763 (1989).
8. Balser, J. R., P. B. Bennett, L. M. Hondeghem, and D. M. Roden. Suppression of time-dependent outward current in guinea-pig ventricular myocytes: actions of quinidine and amiodarone. *Circ. Res.*, **69**:519–529 (1991).
9. Sanguinetti, M. C., and N. K. Jurkiewicz. Two components of cardiac delayed rectifier K^+ current: differential sensitivity to block by class III antiarrhythmic agents. *J. Gen. Physiol.* **96**:195–215, (1990).
10. Roberds, S. L., and M. M. Tamkun. Cloning and tissue-specific expression of five voltage-gated potassium channel cDNAs expressed in rat heart. *Proc. Natl. Acad. Sci. USA* **88**:1798–1802 (1991).
11. Tamkun, M. M., K. M. Knoth, J. A. Walbridge, H. Kroemer, D. M. Roden, and D. M. Glover. Molecular cloning and characterization of two voltage-gated K^+ channel cDNAs from human ventricle. *FASEB J.* **5**:331–337 (1991).
12. Swanson, R., J. Marshall, J. S. Smith, J. B. Williams, M. B. Boyle, K. Folander, C. J. Luneau, J. Antanavage, C. Oliva, S. A. Buhrow, C. Bennett, R. B. Stein, and L. K. Kaczmarek. Cloning and expression of cDNA and genomic clones encoding three delayed rectifier potassium channels in rat brain. *Neuron* **4**:929–939 (1990).
13. Roberds, S. L., and M. M. Tamkun. Developmental expression of cloned cardiac potassium channels. *FEBS Lett.* **284**:152–154 (1991).
14. Boyle, W. A., and J. M. Nerbonne. A novel type of depolarization-activated K^+ current in adult rat atrial myocytes. *Am. J. Physiol.* **260**:H1236–H1247 (1991).
15. Philipson, L. H., R. E. Hice, K. Schaeffer, J. LaMendola, G. I. Bell, D. J. Nelson, D. F. Steiner. Sequence and functional expression in *Xenopus* oocytes of a human insulinoma and islet potassium channel. *Proc. Natl. Acad. Sci. USA* **88**:53–57 (1991).
16. Yellen, G., M. E. Jurman, T. Abramson, and R. MacKinnon. Mutations affecting internal TEA blockade identify the probable pore-forming region of a K^+ channel. *Science* (*Washington D. C.*) **251**:939–942 (1991).
17. Chung, F.-Z., C. D. Wang, P. C. Potter, J. C. Venter, and C. M. Fraser. Site-directed mutagenesis and continuous expression of human β-adrenergic receptors. *J. Biol. Chem.* **263**:4052–4055 (1988).
18. Takeyasu, K., M. M. Tamkun, N. R. Siegel, and D. M. Fambrough. Expression of hybrid (Na^+K^+)-ATPase molecules after transfection of mouse *Ltk*$^-$ cells with DNA encoding the β subunit of an avian brain sodium pump. *J. Biol. Chem.* **262**:10733–10740 (1987).
19. Koren, G., E. R. Liman, D. E. Logothetis, B. Nadal-Ginard, and P. Hess. Gating mechanism of a cloned potassium channel expressed in frog oocytes and mammalian cells. *Neuron* **2**:39–51 (1990).
20. Zagotta, W. N., and R. W. Aldrich. Voltage-dependent gating of *Shaker* A-type potassium channels in *Drosophila* muscle. *J. Gen. Physiol.* **95**:29–60 (1990).
21. MacKinnon, R. Determination of the subunit stoichiometry of a voltage-activated potassium channel. *Nature* (*Lond.*) **350**:232–235 (1991).
22. Armstrong, C. M. Interaction of tetraethylammonium ion derivatives with the potassium channels of giant axons. *J. Gen. Physiol.* **58**:413–437 (1971).
23. Snyders, D. J., P. B. Bennett, and L. M. Hondeghem. Mechanisms of drug-channel interactions, in *The Heart and Cardiovascular System: Scientific Foundations* (H. A. Fozzard, E. Haber, R. B. Jennings, A. M. Katz, and H. E. Morgan, eds.), Raven Press, New York, 2165–2193 (1991).
24. Clay, J. R. Comparison of the effects of internal TEA^+ and Cs^+ on potassium current in squid giant axons. *Biophys. J.* **48**:885–892 (1985).
25. Hartmann, H. A., G. E. Kirsch, J. A. Drewe, M. Taglialatela, R. H. Joho, and A. M. Brown. Exchange of conduction pathways between two related K^+ channels. *Science (Washington D. C.)* **251**:942–944 (1991).
26. Yool, A. J., and T. L. Schwarz. Alteration of ionic selectivity of a K^+ channel by mutation of the H5 region. *Nature (Lond.)* **349**:700–704 (1991).
27. Yellen, G. Permeation in potassium channels: implications for the channel structure. *Annu. Rev. Biophys. Biophys. Chem.* **16**:227–246 (1987).

Send reprint requests to: Dirk J. Snyders, M.D., Stahlman Cardiovascular Research Program, MCN-CC-2209, Vanderbilt University School of Medicine, Nashville, TN 37232-2171.